



UNIVERSITY OF LEEDS

This is a repository copy of *CFD-DNS simulation of irregular-shaped particle dissolution*.

White Rose Research Online URL for this paper:

<http://eprints.whiterose.ac.uk/157390/>

Version: Accepted Version

---

**Article:**

Cao, H, Jia, X [orcid.org/0000-0001-8590-7477](https://orcid.org/0000-0001-8590-7477), Li, Y et al. (2 more authors) (2020) CFD-DNS simulation of irregular-shaped particle dissolution. *Particuology*, 50. pp. 144-155. ISSN 1674-2001

<https://doi.org/10.1016/j.partic.2019.08.003>

---

© 2019 Chinese Society of Particuology and Institute of Process Engineering, Chinese Academy of Sciences. Published by Elsevier B.V. All rights reserved. This manuscript version is made available under the CC-BY-NC-ND 4.0 license <http://creativecommons.org/licenses/by-nc-nd/4.0/>

**Reuse**

This article is distributed under the terms of the Creative Commons Attribution-NonCommercial-NoDerivs (CC BY-NC-ND) licence. This licence only allows you to download this work and share it with others as long as you credit the authors, but you can't change the article in any way or use it commercially. More information and the full terms of the licence here: <https://creativecommons.org/licenses/>

**Takedown**

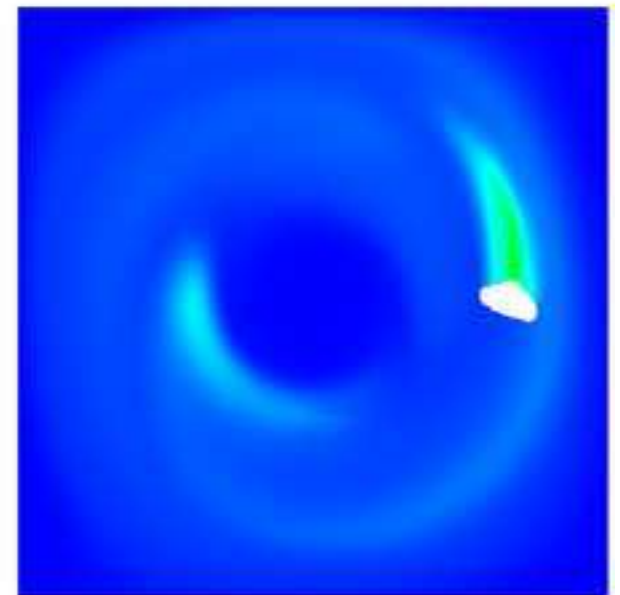
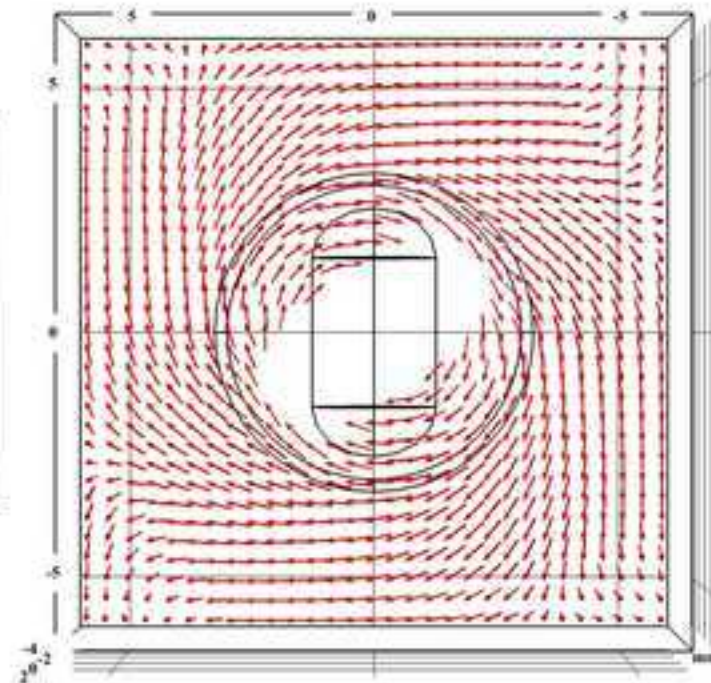
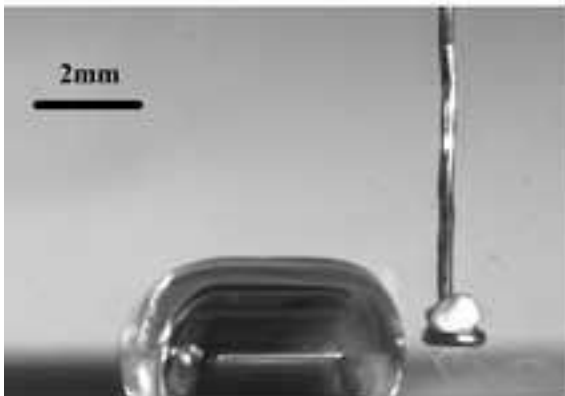
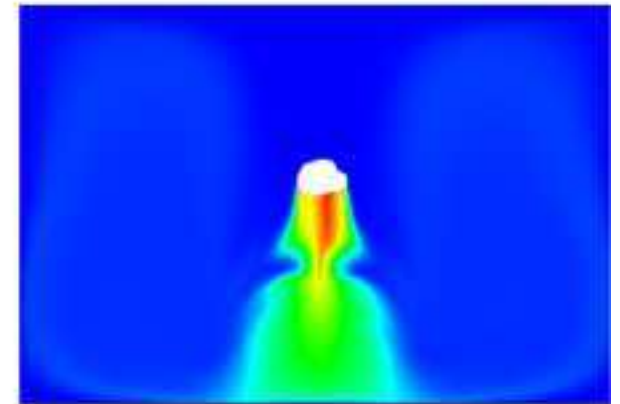
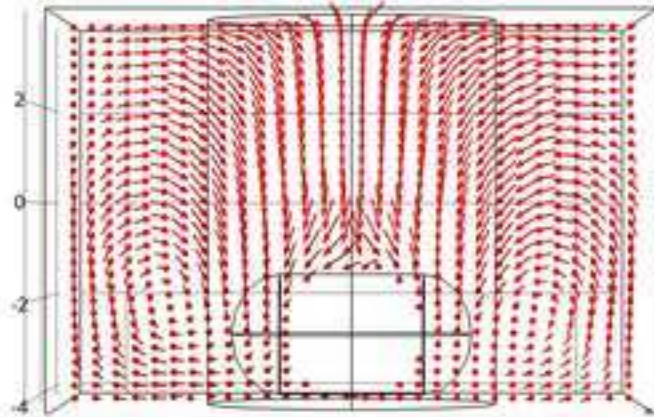
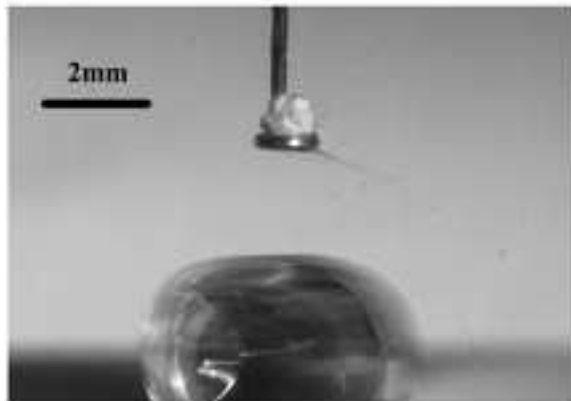
If you consider content in White Rose Research Online to be in breach of UK law, please notify us by emailing [eprints@whiterose.ac.uk](mailto:eprints@whiterose.ac.uk) including the URL of the record and the reason for the withdrawal request.



[eprints@whiterose.ac.uk](mailto:eprints@whiterose.ac.uk)  
<https://eprints.whiterose.ac.uk/>

CFD

DNS



Highlights:

- Irregular shaped particle dissolution is simulated by coupling CFD and DNS.
- Simulation is assessed by experimental data and theoretical prediction.
- Comprehensive agreement has achieved.

# CFD-DNS simulation of irregular shaped particle dissolution

*Hui Cao<sup>1,\*</sup>, Xiaodong Jia<sup>2</sup>, Yongliang Li<sup>1</sup>, Carlos Amador<sup>3</sup> and Yulong Ding<sup>1</sup>*

<sup>1</sup>School of Chemical Engineering, University of Birmingham, B15 2TT, United Kingdom

<sup>2</sup>School of Chemical and Process Engineering, University of Leeds, LS2 9JT, United Kingdom

<sup>3</sup> Proctor & Gamble Newcastle Innovation Centre, Newcastle Upon Tyne, NE12 9TS, United Kingdom

**Corresponding Author** \*h.cao@bham.ac.uk

ABSTRACT A coupling approach between Computational Fluid Dynamics (CFD) and Direct Numerical Simulation (DNS) code DigiDiss has been presented to study the dissolution kinetics of irregular shaped particle in a stirred cuvette. The flow dynamics from CFD was implemented into DigiDiss as initial condition. 3D digital particle structure scanned and reconstructed from X-ray Micro-tomography was used in the simulation. Quantitative assessment of the simulation results was made against experimental data and theoretical prediction through different velocity profile in the vicinity of the particle. The comprehensive agreement demonstrates the coherence of simulation method to reproduce experimental behaviour, which is a step closer to developing a computer software design aide to help with formulation development.

KEYWORDS Single particle dissolution; Computational Fluid Dynamics; Direct Numerical Simulation; X-ray Micro-tomography

## 1. INTRODUCTION

The dissolution kinetics of powders is of critical importance in many industrial and consumer applications, ranging from pharmaceutical and food products, to chemicals, detergents, paints, etc. The study of the dissolution process has been developed in the past century from pure diffusion of single solid solute to convective-diffusion of more complex porous medium, over which the dissolution of particles becomes particularly interesting to nowadays researchers.

### *Diffusion layer-based particulate dissolution models*

The first literature of dissolution theory can be traced back to the end of the 19<sup>th</sup> century, starting with the classic work of Noyes and Whitney [1]. Then Nernst [2] and Brunner [3] reported the *diffusion layer* theory, suggesting a thin layer of stagnant solution forms instantly at the solid-liquid interface during dissolution and diffusion occurs across this layer into the bulk solution. This concept is hydrodynamically unrealistic but allows the complex dissolution process to be analysed in a tractable fashion. The *diffusion layer model*, also called *film model*, is widely used due to its simplicity and applicability to a wide range of dissolution phenomena.

Three classical diffusion-controlled models for monosized spherical particle dissolution under sink conditions are given by:

$$w^{1/3} = w_0^{1/3} - K_{1/3}t \quad K_{1/3} = \left( \frac{4\pi\rho N}{3} \right)^{1/3} \frac{DC_s}{\rho h} \quad (1)$$

$$w^{2/3} = w_0^{2/3} - K_{2/3}t \quad K_{2/3} = \left( \frac{4\pi\rho N}{3} \right)^{2/3} \frac{2DC_s}{\rho} \quad (2)$$

$$w^{1/2} = w_0^{1/2} - K_{1/2}t \quad K_{1/2} = \left( \frac{3\pi\rho N}{2} \right)^{1/2} \frac{DC_s}{k'\rho} \quad (3)$$

where  $w$  is the particle weight at time  $t$ ,  $w_0$  is the initial particle weight,  $K_{1/3}$ ,  $K_{1/2}$  and  $K_{2/3}$  are composite rate constants,  $\rho$  is the density of the particle,  $N$  is the number of particles,  $D$  is the diffusion coefficient,  $C_s$  is the solubility,  $h$  is the diffusion layer thickness,  $k'$  is a constant.

Eq. (1) is known as the cube-root law reported by Hixson and Crowell [4, 5]. It was derived based on the assumption that dissolution rate is proportional to the surface area of spherical particles. It is appropriate when particle size is much larger than the diffusion layer thickness. Eq. (2) has a two-thirds-root dependency on weight and it applies when the particle size is much smaller than the diffusion layer thickness [6, 7]. Eq. (3) has a square-root dependency on weight reported by Niebergall et al. [8], and it is intermediate between cube-root and two-thirds-root models.

#### *Convective-diffusion based particulate dissolution models*

In most of the scenarios, particles dissolve nonstationary. The general convective-diffusion in three dimensions is given:

$$\frac{\partial C}{\partial t} = D \left( \frac{\partial^2 C}{\partial x^2} + \frac{\partial^2 C}{\partial y^2} + \frac{\partial^2 C}{\partial z^2} \right) - v_x \frac{\partial C}{\partial x} - v_y \frac{\partial C}{\partial y} - v_z \frac{\partial C}{\partial z} \quad (4)$$

where  $v_x$ ,  $v_y$ , and  $v_z$  are liquid velocities in the  $x$ -,  $y$ -, and  $z$ -directions in Cartesian coordinates. With the velocity function, the convective diffusion model is more hydrodynamically realistic, and it is more accurate to predict dissolution rate. However, it is usually complicated to describe the fluid dynamics accurately. A simple way is to derive Eq. (4) with fluid dynamic parameters from a spherical particle. Levich reported an expression for mass transport to a free-falling sphere:

$$w^{5/9} = w_0^{5/9} - 2.35 \cdot C_s D^{2/3} v^{1/3} \rho^{-4/9} t \quad (5)$$

where  $v$  is the terminal velocity of the free-falling sphere relative to the bulk solvent velocity [9].

Dimensionless number Sherwood number (Sh) is a popular replacement of the velocity in the above model particularly when Reynolds number (Re) and Schmidt number (Sc) are readily available. Models can be found in [10-17] and have been validated through both single particle and bulk particles dissolution experiment.

#### *Dissolution of single particle*

The dissolution kinetics of particles is usually conducted on a single particle or bulk particles. Due to industry preference, bulk particle dissolution has been investigated with various quantitative analytical techniques such as conductivity measurement [17], UV-Vis spectrometry [18], laser diffraction PSD analyser [19], and the combination of them [20]. However, these techniques require high amount of sample preparation and the total measurement error is determined by the inherent error in every step of the sampling chain [21, 22]. Furthermore, particles have different interior/surface structure, and it is difficult to measure their dissolution

rate using bulk methods as it will be averaged between particles. Studying single particle dissolution behaviour has its unique advantages such as minimising the chemical analytical required the particle amount, shortening sampling chain, and also validating mathematical models more accurately.

The study of individual particle dissolution has been investigated mainly through imaging based particle morphology monitoring approach [23-27]. This technique has been widely used in chemical engineering and pharmaceutical science [23, 28-30]. The first assessment of this technique was reported by Marabi et al [23]. They used optical microscope to acquire single particle dissolution images and analysed these images to obtain dissolution rate constant by fitting their experiment data to a shrinking sphere model. The constant showed a linear correlation to the reciprocal of the viscosity, following the Einstein-Stokes equation, and so that the authors concluded optical microscopy technique is a feasible approach to study single particle dissolution. A more comprehensive study was reported by Svanbäck et al. to further evaluate this technique by comparing dissolution results from image analysing with chemical analytical results (UV spectrophotometry results) [26]. Across the three different but highly spherical particles that were investigated, they found a  $98\pm 1\%$  agreement between physical and chemical dissolution data. Consequently, they concluded that image analyse can be used as a viable analytical technique in single-particle dissolution studies. This technique has shown great potential in particle dissolution related scenarios. Börjesson et al flew individual sodium caseinate particle through a confined cell, monitored particle dissolution behaviour using an optical microscope, and found a large variance in dissolution rate between particles which might relate to particle lumps formation problem during powder reconstitution in food industry [24]. Hassenkam et al. experimentally investigated single coccolith dissolution in different pH value

ocean water by visualizing particle morphology at different time laps and revealed the consequence of rising CO<sub>2</sub> level in atmosphere and its effect on marine organisms [25]. Recently, automated image analysis technique has been implemented in particle size monitoring which can provide real-time characterization of particle dissolution behaviour [27].

Apart from experimental study, mathematic models and numerical simulation approaches have also developed over the years. Effort has been focused on implementing more parameters into the three classic equations (Eq. (1), (2), (3)) such as particle shape factor [31, 32], particle size distribution [31, 33], and individual solubility, diffusion layer thickness and dissolution rate [31, 33-35]. For example, Pedersen and Brown considered the particle size distribution in their computer model, and found that the cube-root model worked best with the smallest mean squared deviation for the fitted curve [31]. However, they also found the fitting results of the cube-root and the square-root models were almost equally good. Similar results can be found in [32-34, 36, 37]. Dali and Carstensen incorporated a semi-empirical shape factor to the cube-root equation, and found out the shape factor was not constant but rather a changeable value as particle dissolves [32]. In recent years, nanoparticles have been widely applied in the pharmaceutical industry particularly for poorly water-soluble drugs. The increase in specific surface area that comes with a decrease in particle size offers an enhanced dissolution rate for these valuable drugs, which brings new challenges for dissolution models. A comprehensive mathematical model, developed by Horkovics-Kovats [34] based on the root-laws theory, can predict polydisperse and polymorphic nanoparticle dissolution kinetics with increased nanoparticle solubility. The model can also describe the effect of Ostwald ripening: the transition of metastable polymorphic form into a more stable crystalline form (lower solubility). More mathematical modelling of drug dissolution was published in a review paper [38].

It is usually complicated to apply convective-diffusion to derive accurate expressions for solid dissolution because of the need to describe the fluid dynamics accurately. Highly resolved numerical simulations are a way of revealing the complex physical interactions between the solid and the liquid phase: the flow dynamics control mass transfer rates; mass transfer results in solute concentration gradients in the liquid phase that may have impact on the flow dynamics, e.g. through local variations in the liquid viscosity. The flow dynamics can be precisely solved by Computational Fluid Dynamics (CFD) or Lattice-Boltzmann Method (LBM), whereas the mass transfer of solid particles can be governed by the Noyes-Whitney equation and coupled to the flow dynamics. The research in this particular area has been actively centralized in several groups world widely. Štěpánek and his group developed their own numerical algorithm to create digital granules and simulate the dissolution kinetics [18, 19, 39-43]. They studied the dissolution behaviour of granules and linked their structure obtained from X-ray Microtomography (XMT) with their dissolution behaviour. By comparing simulation results to experiment data, they stated that their model can predict granule dissolution process qualitatively. Their recent work shows higher accuracy when compared simulation results to analytical data (particle size detected from laser diffraction and solution concentration analysed by UV-Vis) [18, 19]. Similarly, Jia and his co-workers reported a code *DigiDiss*, based on direct numerical simulation (DNS), to simulate irregular shaped particles dissolving in any hydrodynamic conditions [44-46]. They use digital particle structures scanned from XMT and the simulation precision mainly depends on scanning resolution. They recently implemented LBM for simulating flow dynamics and achieved good agreement in drag coefficient with experimental data or empirical correlations [46]. Derksen and co-workers developed LBM code for simulating spherical particles dissolving in laminar flow [16, 47, 48]. Other models were also

reported for different specialities for example Babenko et al. developed a mathematical model for the dissolution of a single spherical particle considering the effect of nonstationarity at the initial stage of dissolution and the influence of movement of the phase boundary [49].

The aim of this paper is to assess a new coupling approach to simulate dissolution kinetics of irregular shaped particle based on code *DigiDiss*. CFD was used to simulate flow dynamics of water in a cubic cuvette with a magnetic stir and a stationary particle, and the results were implemented to *DigiDiss* as initial condition for the same particle to dissolve. Simulation results were compared with experimental data acquired through optical imaging process and theoretical equations. Different case study were investigated e.g. rotating speed, particle position in the covette.

## **2. MODEL DESCRIPTION**

### **2.1 Simulation in COMSOL**

COMSOL Multiphysics Rotating Machinery, Laminar Flow module is used to first calculate the velocity distribution of stirring tank. The Rotating Machinery in COMSOL CFD module allows moving rotating parts in stirred tanks, mixers and pumps etc. It formulates the Navier-Stokes equations in a rotating coordinate system. Parts that are not rotated are expressed in the fixed material coordinate system. The rotating and fixed parts are coupled together by an identity pair, where a flux continuity boundary conditions is applied.

Figure 1 shows the geometry of the model. The geometry is divided into two parts. The outer cylinder is the fixed part. The inner cylinder with surface boundaries of a magnetic stir is the rotating part, which rotates counter clockwise at a speed of 100, 200 and 300 rpm. Navier-Stokes equations formulates both in the rotating frame in the inner domain and the fixed coordinated in

the outer one. Between outer domain and inner domain, walls are assembled as identity pair. All the other walls are set as non-slip boundary conditions including the surfaces of the magnetic stir. Water property is applied through the whole domain. Numerical mesh size between 0.02 mm and 0.05 mm is applied. The fully developed velocity field inside the whole domain is exported as text file and imported into DigiDiss as initial condition.

**Figure 1.** Geometry of the cuvette with a magnetic stir.

## 2.2 Simulation in *DigiDiss*

Mass balance is the fundamental mechanism in mass transfer problems. The governing equations for dissolution in DigiDiss are:

$$\frac{\partial C}{\partial t} + (u_x \frac{\partial C}{\partial x} + u_y \frac{\partial C}{\partial y} + u_z \frac{\partial C}{\partial z}) = D(\frac{\partial^2 C}{\partial x^2} + \frac{\partial^2 C}{\partial y^2} + \frac{\partial^2 C}{\partial z^2}) \quad (6)$$

$$\frac{dW}{dt} = -KA(C_s - C) \quad (7)$$

Eq. (6) is the convection-diffusion equation [50] which describes the concentration distribution in a liquid.  $C$  is the mass concentration ( $\text{kg m}^{-3}$ ),  $t$  is the time (s),  $(u_x, u_y, u_z)$  is fluid velocity components ( $\text{m s}^{-1}$ ),  $D$  is the diffusivity ( $\text{m}^2 \text{s}^{-1}$ ) and  $(x, y, z)$  is the spatial coordinates (m). At the solid/liquid interface, Eq. (7) known as the Noyes-Whitney equation is applied. In Eq. (7),  $W$  is the weight of the dissolved solid (kg),  $K$  is the dissolution constant ( $\text{m s}^{-1}$ ),  $A$  is the surface area of solid exposing to solvent ( $\text{m}^2$ ), and  $C_s$  is the solubility or saturation concentration of the solid ( $\text{kg m}^{-3}$ ). A schematic of the code is described in Figure 2 which illustrates the discretization of Eq. (6) based directly on mass balance, Fick's first law (first equation in Figure

2) and the Noyes-Whitney equation (second equation in Figure 2) in a lattice grid cell.  $\Delta x$  is the cell width (m).

**Figure 2.** Schematics of mathematical formulation for dissolution[44].

For the transient mode, the following equations can be written explicitly [44]. The equations state that the rate of change in mass for a particular component in the fluid cell is the sum of gains and losses of mass due to convection, diffusion and dissolution, on each of the six sides of the cell (in 3D) [44]:

$$\begin{aligned}
 & V \frac{C^{t+\Delta t} - C}{\Delta t} = && \text{mass increase rate} \\
 & +uc_x A + uc_y A + uc_z A && \text{convection in X, Y, Z} \\
 & +K_{i-1} A(C_{i-1}^s - C) + K_{i+1} A(C_{i+1}^s - C) && \text{dissolution in X} \\
 & +K_{j-1} A(C_{j-1}^s - C) + K_{j+1} A(C_{j+1}^s - C) && \text{dissolution in Y} \\
 & +K_{k-1} A(C_{k-1}^s - C) + K_{k+1} A(C_{k+1}^s - C) && \text{dissolution in Z} \\
 & +DA \left( \frac{C_{i-1} - C}{\Delta x} + \frac{C_{i+1} - C}{\Delta x} \right) && \text{diffusion in X} \\
 & +DA \left( \frac{C_{j-1} - C}{\Delta x} + \frac{C_{j+1} - C}{\Delta x} \right) && \text{diffusion in Y} \\
 & +DA \left( \frac{C_{k-1} - C}{\Delta x} + \frac{C_{k+1} - C}{\Delta x} \right) && \text{diffusion in Z} \\
 & V = (\Delta x)^3 \quad A = (\Delta x)^2 \quad \Delta x = \Delta y = \Delta z \\
 & uc_x = \begin{cases} |u_x|(C_{i-1} - C) & \text{if } u_x > 0 \\ |u_x|(C_{i+1} - C) & \text{if } u_x < 0 \end{cases} \\
 & uc_y = \begin{cases} |u_y|(C_{j-1} - C) & \text{if } u_y > 0 \\ |u_y|(C_{j+1} - C) & \text{if } u_y < 0 \end{cases} \\
 & uc_z = \begin{cases} |u_z|(C_{k-1} - C) & \text{if } u_z > 0 \\ |u_z|(C_{k+1} - C) & \text{if } u_z < 0 \end{cases}
 \end{aligned} \tag{8}$$

The unique advantage of DigiDiss is the capability of importing real particle structure scanned by XMT into the model, which is also described in a lattice grid. Figure 3 (a) is the geometry of an anhydrous  $\text{Na}_2\text{CO}_3$  granule scanned by XMT. This geometry was placed inside the cuvette at two positions, one on top of the magnetic stir (see Figure 3 (b)), the other one beside the stir (see Figure 3 (c)). Particle position was controlled by restricting the distance from particle geometry centre to either the centre of the stir, or the tip edge of the stir in the two cases, which are the same distances applied in experiment. In Figure 3 (b) and (c), the irregular shaped object represents the particle. The black box around the particle represents water domain. Solid wall is used as domain boundary condition throughout the simulation. The computing precision and the balance between time scale, model pixel numbers and steady state are explained in previous paper [44]. Velocity distribution calculated by COMSOL was imported into the model as initial flow condition.

**Figure 3.** Digital particle in water domain: (a) on top of the stir and (b) beside the stir.

### **3. EXPERIMENT**

#### **3.1. Material**

Anhydrous non-porous  $\text{Na}_2\text{CO}_3$  powder was purchased from Sigma-Aldrich and used as sample particle in this work. Deionised water was used for particle dissolution test.

#### **3.2. Particle characterization**

Particle surface morphology was analysed with a Scanning Electron Microscope (SEM) (Hitachi TM3030, U.S.A) operated at 15 kV in low vacuum mode and equipped with a backscatter detector. Magnification was set as  $\times 100$  and  $\times 1500$  in the scanning.

XMT (Phoenix Nanotom NF160, GE) was used to scan the particles at resolutions 1–9  $\mu\text{m}$  per voxel. The scans were carried out with 80-100 kV and 50-100  $\mu\text{A}$  X-ray settings and a scan step of  $0.25^\circ$  per projection. The 1440 projections were reconstructed using Phoenix reconstruction software for the three dimensional structure. Such three dimensional data were then processed using an in-house software program (*DigiUtility*) to scale down to a suitable voxel size to be accommodated into *DigiDiss* for dissolution simulation. As mentioned in previous paper [51] understanding errors in spatial modelling may be of critical importance in accuracy of simulation. Both X-ray scan and pixel processing followed could give rise to errors to the original samples. Boundaries composed of pixels may have errors within one pixel length. To achieve more presentable models scanning resolutions at a lower micrometre were used. The digitised 3D structure was then read into *DigiDiss*.

### **3.3. Dissolution test**

A high speed camera (FASTCAM SA 5, Photron Ltd) with a macro lens was used to focus on the single particle inside a transparent cubic cuvette. The size of the cuvette is  $15\text{ mm} \times 15\text{ mm} \times 15\text{ mm}$ . First, 1.2 mL deionized water was added into the cuvette and the magnetic stir was switched on. Then particle was loaded into a holder made by copper wire to sit the particle. The wire was attached to a step motor to control the position of the particle inside cuvette. The dissolution started immediately when the particle touched water. Before dissolution process totally finished, the particle fell off the wire due to gravity and the drag force from the swirling water. High speed camera captured the whole process by 500 frame per second and the video was analysed by ImageJ to extract the information of particle shape changing as a function of time. Figure 4 shows the dissolution experiment set up of a single particle sitting on the wire and positioned at the two investigated positions (a) on top of the stir and (b) beside the stir.

**Figure 4.** Dissolution experiment of a single particle at different position (a) on top of the stir and (b) beside the stir.

## 4. RESULTS AND DISCUSSION

### 4.1. Particle characterization

The surface morphology of anhydrous  $\text{Na}_2\text{CO}_3$  granules are shown in Figure 5 (a) and (b) at 100 and 1500 times magnifications respectively. The granule has irregular external shape with a rough surface. Amount of pebble looking small granules (less than  $20\ \mu\text{m}$ ) attach on the surface. Figure 5 (c) is the digitalised three dimensional structure of the granule which was scanned and reconstructed by XMT.

**Figure 5.**  $\text{Na}_2\text{CO}_3$  granules characterization: (a) SEM image at  $\times 100$  magnification, (b) SEM image at  $\times 1500$  magnification, and (c) digitalised three dimensional model of the granule from XMT.

### 4.2. Dissolution experiment

Image sequences from high speed camera are shown in Figure 6 where  $\text{Na}_2\text{CO}_3$  granule sits on top of the magnetic stir with a distance of 2.4 mm between the sample holder and the stir. In this case, the granule was located in the middle of swirling flow. The sample holder was driven to the position by a step motor. Once contacting with water, dissolution started immediately before the sample holder arrived at the pre-set position. As a result, two aspects were carried out to guarantee the analyse was consistent. First, the particles were initially larger than 1 mm in diameter which gives it some time to travel to the position before the starting point of analysing. Second, the images with particle size of 1 mm in diameter was selected as the starting point (time zero). One can see from the images that as the dissolution process continued, the solid part diffused into water, formed a layer in the local area, then the solution was carried away by the agitated fluid leaving a “tail” below the granule. The granule stabilized on the sample holder for

116 s (from time 0 point), and was blown away by the fluid. The surface area of particle as a function of time was used to represent the release behaviour. Result shows that 93 % of the total weight is reduced during this time period.

**Figure 6.** Image sequences from high speed camera video of  $\text{Na}_2\text{CO}_3$  granule dissolves on top of magnetic stir. All images share the same scale bar.

Comparable experiment of  $\text{Na}_2\text{CO}_3$  granule sitting beside the stir are shown in Figure 7. In this case, the granule was probed to experience higher shear than the above case. The same starting point is selected for analysing. The distance between the tip of stir and the sample holder is 0.8 mm. Similar to the above case, the granule stabilized on the sample holder initially. However, after dissolving 90 s (from time 0 point), particle was blown away from the holder, which is 16 s faster. Result shows that 93 % of the total weight is reduced.

**Figure 7.** Image sequences from high speed camera video of  $\text{Na}_2\text{CO}_3$  granule dissolves beside magnetic stir. All images share the same scale bar.

#### 4.3. COMSOL simulation

Agitation plays an important role in dissolution. This is mainly due to the shear flow around particles which accelerates the transport of solute to the bulk of solvent. Figure 8 shows COMSOL simulation results of velocity distribution inside the cuvette after agitating for 10 s with a rotating speed of 100 rpm at 20 °C. Blue colour represents low value, and red colour represents high value. The whole velocity magnitude distributes from 0 to 0.0314 m/s. In most of the area far away from the stir, for example near the water surface or the corner on the cuvette bottom, the velocity is nearly 0. The closer to the stir, the higher the velocity. At the very close position, for example the circle where the tips of the stir pass through, velocity magnitude is significantly higher than other positions. At the point 2.4 mm on top of the stir, which was the

first investigated position in experiment, velocity is about 0.004 ~ 0.006 m/s. While at the point 0.8 mm away from the stir tip horizontally (the second investigated position in experiment), the velocity is between 0.008 and 0.012 m/s, showing nearly two times higher than the first case. The velocity distribution within the dissolution cuvette revealed detail information about the velocity of water around particle, which was taken for later numerical calculation of particle dissolution profile. The flow vector images (Figure 8 (c) and (f)) show that the magnetic stir drives water in the radial direction. On the position where particle sits on top of the stir, fluid is directed downwards. While beside the stir, fluid pass through particle in the radial direction. These results imply that the dissolved solid would be carried away downwards the stir in the first case, and axisymmetrically in the second case.

**Figure 8.** COMSOL simulation results of velocity distribution in XY plane (a) 3D and (b) 2D, and YZ-plane (d) 3D and (e) 2D at 100 rpm 20 °C. (c) and (f) are arrow display of flow direction at XY plane and YZ plane.

#### 4.4 Simulation in DigiDiss

The velocity field from COMSOL was imported into DigiDiss to simulate particle dissolution hydrodynamically. The geometry in two simulation approaches are identical, however, the numerical mesh types are different. In DigiDiss, structured grid hexahedron was chosen in 3D model. The mesh type in COMSOL was tetrahedron. When coupling the velocity field between these two, regular structured grid was selected in COMSOL for output in order to match the grid in DigiDiss.

Figure 9 shows the velocity field in DigiDiss after importing from COMSOL, (a) is the 3D view, (b) is the XY-plane and (c) is the YZ-plane, which corresponds to XY- and YZ-planes in Figure 8. Blue colour represents low velocity, red colour is high velocity, and others are in between. The

flow pattern in DigiDiss shows similar trends as in COMSOL. The colour legend in Figure 9 is slightly different from Figure 8. This is mainly due to mesh distribution difference between these two codes and also the set up of colour legend. Minor numerical errors might bring into simulation results.

**Figure 9.** Velocity field in DigiDiss (a) 3D view (b) XY-plane and (c) YZ-plane.

After importing the velocity field, 3D digital structure of  $\text{Na}_2\text{CO}_3$  granule scanned from XRT was imported to the investigated positions in experiment. The simulation results of granule concentration map are shown in Figure 10 where colour spectrum red to blue indicates high to low concentration. The images demonstrate that as dissolution goes on, the remaining structures become significantly smaller than the original geometries. The flow field results from COMSOL indicate that particle experiences different flow vector in experiment. When particle sits on top of the stir, Figure 11 (a) to (c) show coherent concentration development as the flow field distribution: (a) the dissolved part being carried away from the particle and towards the stir, then (b) continuously carried around the stir towards the cuvette walls and finally (c) distributing in the whole cuvette with much less on top of the stir along the axis. In the second case when particle sits beside the stir, similar phenomena have been observed. From (d) to (f), the top views of concentration map show that the dissolved part is continuously carried away by the fluid axisymmetrically until the end of the dissolution.

**Figure 10.**  $\text{Na}_2\text{CO}_3$  granule concentration map at early stage (less than 0.1 wt % released), 50 wt % released and 100 wt % released when it is on top of stir (a), (b), (c) (YZ-plane in **Figure 8**), and beside stir (d), (e), (f) (XY-plane in **Figure 8**) respectively. Rotating speed of the stir is 100 rpm.

The release fraction of particle by weight is plotted in Figure 11 for agitating speeds of 100, 200 and 300 rpm. The results suggest that for both two positions, as agitating speed increases, dissolution becomes faster. From 100 to 300 rpm, particle finishes from 188 s to 165 s on top of

the stir, and 134 s to 123 s beside the stir. Particle dissolves significantly faster beside the stir than on top of it, resulting in 29 %, 28 % and 25 % shorter total dissolution time at 100, 200 and 300 rpm respectively. COMSOL simulation results have revealed that the stir has consistently generated higher average velocity around the particle beside the stir than on top of it.

**Figure 11.** DigiDiss simulation results of particle dissolution behaviour in different agitating speed when particle is located (a) on top of the stir and (b) beside it.

#### 4.5 DigiDiss validation

Dissolution is a molecular level process and critically dependent on exposed surface area. It is well known that surface area obtained from digital imaging is different from (usually much lower than) its true value [52] and the difference is resolution dependent. To validate the DigiDiss model as well as the approach of coupling COMSOL velocity into it, simulation results were compared to experiment results and theoretical calculation at 100 rpm with different particle positions.

Sherwood number ( $Sh$ ) is introduced to represent the ratio of convective to diffusive mass transport:

$$Sh = \frac{K \cdot L}{D} \quad (9)$$

where  $L$  is the characteristic length (m). The mass transfer coefficient for a spherical particle can be written as:

$$K = \frac{Sh \cdot D}{d_{p,t}} \quad (10)$$

where  $d_{p,t}$  is the particle diameter (m) at dissolution time  $t$  (s).

Assuming particle is homogeneous, and density  $\rho_p$  ( $\text{kg m}^{-3}$ ) is constant throughout dissolution,

the initial mass of particle  $W_0$  (kg) is:

$$W_0 = \rho_p \cdot \frac{1}{6} \cdot \pi \cdot d_{p,0}^3 \quad (11)$$

where  $d_{p,0}$  is the initial particle diameter (m). So the remaining mass of particle  $W_t$  (kg) at time  $t$  can be expressed as:

$$W_t = \rho_p \cdot \frac{1}{6} \pi \cdot d_{p,t}^3 = M_0 \cdot \left( \frac{d_{p,t}}{d_{p,0}} \right)^3 \quad (12)$$

$$\text{Hence } d_{p,t} = d_{p,0} \cdot \left( \frac{W_t}{W_0} \right)^{1/3} \quad (13)$$

Similarly, the total surface area  $A_t$  ( $\text{m}^2$ ) of the particle exposing to solvent at time  $t$  can be given by

$$A_t = \pi \cdot d_{p,t}^2 = \pi \cdot d_{p,0}^2 \left( \frac{W_t}{W_0} \right)^{2/3} = A_0 \cdot \left( \frac{W_t}{W_0} \right)^{2/3} \quad (14)$$

where  $A_0$  is the initial surface area of particle ( $\text{m}^2$ ).

Substituting Eq. (7) with Eq. (10) and (14), and assuming  $C \ll C_s$ , Sherwood number can be introduced to the Noyes-Whitney equation which gives a root-law:

$$\frac{dW_t}{dt} = -\frac{Sh \cdot D}{d_{p,t}} \cdot A_t \cdot C_s = -\frac{Sh \cdot D}{d_{p,0}} \cdot A_0 \cdot C_s \cdot \left(\frac{W_t}{W_0}\right)^{1/3} \quad (15)$$

Many different expressions have been developed to calculate the Sherwood number for a spherical particle that work well under different assumptions. When particles have higher density than the fluid, the following expression can be used [53]:

$$Sh = 2 + 0.44 \cdot \left(\frac{\rho_f \cdot u \cdot d_p}{\mu_f}\right)^{0.5} \cdot \left(\frac{\mu_f}{\rho_f \cdot D}\right)^{0.38} \quad (16)$$

where  $\rho_f$  is the solvent density ( $\text{kg m}^3$ ),  $\mu_f$  is the solvent viscosity, and  $u$  is the relative velocity ( $\text{m s}^{-1}$ ) between liquid and particle [14].

Eq. (15) was solved by commercial software package (MATLAB 7.1, The MathWorks Inc., Natick, MA, 2000). Theoretical results were compared to image analyse results from dissolution experiment and DigiDiss analytical results, showing in Figure 12 as case study of 100 rpm.

In the two particle positions investigated, acceptable agreements among theory, DigiDiss and experiment have been achieved. Experiment shows lower release rate than the other two in the early stage, and later developed to higher release rate. The trends from experiment in later stage implies a much faster dissolution time than predicted from both theory and DigiDiss. To accurately compare the differences, the time point when particle lost 93 % weight was chosen, which was the time point when particle was blown away from the holder in experiment. The horizontal black dot line in both Figure 12 (a) and (b) indicates this time point. At 93 % weight loss when particle was on top of the stir, the time for experiment was 116 s, for theory was 130 s and for DigiDiss was 129 s. When particle was beside the stir at point 93 %, the time for

experiment was 90 s, for theory was 110 s and for DigiDiss was 95 s. The results from DigiDiss show better agreement to experiment result than theoretical prediction. Such a result indicates that DigiDiss is capable of predicting complex convection dissolution with assistance of external fluid velocity field which can be simulated by CFD method.

**Figure 12.** Comparing result of experiment, DigiDiss simulation and Eq. (15) for  $\text{Na}_2\text{CO}_3$  granule locating (a) on top of and (b) beside the magnetic stir for 100 rpm.

#### 4.6 Discussion

With the information of local velocity around particles, Eq. (15) could be one efficient approach to predict particle dissolution behaviour in a flow regime. On the other hand, DigiDiss has shown its unique advantages, including using real particle morphology (XMT structure) in simulation without damaging the particle.

Although acceptable agreements have been achieved, several aspects could be addressed in the future to further improve the predicting quality. The couple between DigiDiss and COMSOL was a simplified approach, only the steady-state velocity from COMSOL was used as initial flow field in DigiDiss. However, as dissolution continued, velocity in reality changed dynamically, and this was not implemented in DigiDiss in the present model. At each lattice grid, velocity remained as the initial imported value. A real-time coupling between DigiDiss and COMSOL while exchanges velocity value at each time step can overcome this through modifying DigiDiss code. Another benefit through the real-time coupling is the capability to take into account local viscosity/density effect on convective dissolution. For example, since the velocity from COMSOL is implemented into DigiDiss as initial flow field, after the first time step in DigiDiss, the concentration changes in each lattice grid can be implemented into COMSOL as new fluid property (density, viscosity etc.) for next step calculation. With these new information,

COMSOL can calculate flow field more precisely and the velocity can be implemented into DigiDiss to calculate the next dissolution step. As so on, the real-time coupling can significantly improve simulation accuracy but probably longer computing time. An alternative worth pursuing is to make LBM within *DigiDiss* [46]. That way, flow dynamics and mass transfer coupling would be much easier. It will also be applicable to cases when the wire/particle is too large to ignore. Wire/particle is ignored in COMSOL flow calculation at present. Further validation can be conducted accordingly.

Optical image analysing approach brings high deviation into experiment results. An in situ measurement such as light scattering, UV-Vis spectrum or laser diffraction [19] can potentially improve experiment results much more accurately to further validate the present model. In the experiment, particle did not disintegrate. However, disintegration is highly possible to occur for porous particle dissolving in different conditions, including no/low/high shear flow. A more rigorous, physics based model is required in order to predict disintegration in DigiDiss, rather than stochastic process in the current code.

#### **4. CONCLUSIONS**

A new coupling approach is proposed to simulate convective dissolution kinetics of irregular shaped particle based on DNS code *DigiDiss*. Flow dynamics of water was simulated in CFD for a cubic cuvette with a magnetic stir and a stationary particle, and the results were implemented to *DigiDiss* as initial condition for the same particle to dissolve. This approach was assessed with experimental dissolution data and a convective-diffusion equation based on the cubic-law theory. The different case studies, e.g. rotating speed, particle position in the covette, show comprehensive agreement between this approach and experimental results, suggesting that

DigiDiss is capable of predicting complex convective dissolution for irregular shaped particles with implemented fluid dynamics from CFD.

## ACKNOWLEDGMENT

The authors would like to give their acknowledgement to Proctor & Gamble Ltd., Newcastle Technical Centre for the research support.

## REFERENCES

1. Noyes, A.A. and W.R. Whitney, THE RATE OF SOLUTION OF SOLID SUBSTANCES IN THEIR OWN SOLUTIONS. *Journal of the American Chemical Society*, 1897. **19**(12): p. 930-934.
2. Nernst, W., Theorie der Reaktionsgeschwindigkeit in heterogenen Systemen. *Z. Phys. Chem.*, 1904. **47**: p. 52-55.
3. Brunner, E., Reaktionsgeschwindigkeit in heterogenen Systemen. *Z. Phys. Chem.*, 1904. **43**: p. 56-102.
4. Hixson, A.W. and J.H. Crowell, Dependence of Reaction Velocity upon surface and Agitation I-Theoretical Consideration. *Industrial & Engineering Chemistry*, 1931. **23**(8): p. 923-931.
5. Hixson, A.W. and J.H. Crowell, Dependence of Reaction Velocity upon surface and Agitation II-Experimental Procedure in Study of Surface. *Industrial & Engineering Chemistry*, 1931. **23**(9): p. 1002-1009.
6. Higuchi, W.I. and E.N. Hiestand, Dissolution Rates of Finely Divided Drug Powders I: Effect of a Distribution of Particle Sizes in a Diffusion-Controlled Process. *Journal of Pharmaceutical Sciences*, 1963. **52**(1): p. 67-71.
7. Higuchi, W.I., E.L. Rowe, and E.N. Hiestand, Dissolution Rates of Finely Divided Drug Powders II: Micronized Methylprednisolone. *Journal of Pharmaceutical Sciences*, 1963. **52**(2): p. 162-164.
8. Niebergall, P.J., G. Milosovich, and J.E. Goyan, Dissolution Rate Studies II. *Journal of Pharmaceutical Sciences*, 1963. **52**(3): p. 236-241.
9. Levich, V.G., *Physicochemical hydrodynamics*. 1962, Englewood Cliffs, N.J.: Prentice-Hall.
10. Hixson, A.W. and S.J. Baum, Agitation. Mass Transfer Coefficients in Liquid-Solid Agitation Systems. *Industrial & Engineering Chemistry*, 1941. **33**(4): p. 478-485.
11. Hixson, A.W. and S.J. Baum, Agitation. Performance of Propellers in Liquid-Solid Systems. *Industrial & Engineering Chemistry*, 1942. **34**(1): p. 120-125.
12. Hixson, A.W. and S.J. Baum, Mass Transfer and Chemical Reaction in Liquid-solid Agitation. *Industrial & Engineering Chemistry*, 1944. **36**(6): p. 528-531.
13. Harriott, P., Mass transfer to particles: Part I. Suspended in agitated tanks. *AIChE Journal*, 1962. **8**(1): p. 93-101.

14. Levins, D.M. and Glastonb.Jr, Particulate-Liquid Hydrodynamics and Mass-Transfer in A Stirred Vessel. 2. Mass-Transfer Transactions of the Institution of Chemical Engineers and the Chemical Engineer, 1972. **50**(2): p. 132-&.
15. Basmadjian, D., Mass Transfer: Principles and Applications. 2003, USA: CRC Press.
16. Hartmann, H., J.J. Derksen, and H.E.A. van den Akker, Numerical simulation of a dissolution process in a stirred tank reactor. Chemical Engineering Science, 2006. **61**(9): p. 3025-3032.
17. Cao, H., et al., A modelling framework for bulk particles dissolving in turbulent regime. Chemical Engineering Research and Design, 2016. **114**(Supplement C): p. 108-118.
18. Kašpar, O., et al., Combined UV/vis and micro-tomography investigation of acetaminophen dissolution from granules. International Journal of Pharmaceutics, 2013. **458**(2): p. 272-281.
19. Smrčka, D., J. Dohnal, and F. Štěpánek, Dissolution and disintegration kinetics of high-active pharmaceutical granules produced at laboratory and manufacturing scale. European Journal of Pharmaceutics and Biopharmaceutics, 2016. **106**: p. 107-116.
20. Mitrano, D.M., et al., Tracking dissolution of silver nanoparticles at environmentally relevant concentrations in laboratory, natural, and processed waters using single particle ICP-MS (spICP-MS). Environmental Science: Nano, 2014. **1**(3): p. 248-259.
21. Alsenz, J. and M. Kansy, High throughput solubility measurement in drug discovery and development. Advanced Drug Delivery Reviews, 2007. **59**(7): p. 546-567.
22. Paakkunainen, M., et al., Uncertainty in dissolution test of drug release. Chemometrics and Intelligent Laboratory Systems, 2009. **97**(1): p. 82-90.
23. Marabi, A., et al., Assessing dissolution kinetics of powders by a single particle approach. Chemical Engineering Journal, 2008. **139**(1): p. 118-127.
24. Börjesson, E., et al., The dissolution behavior of individual powder particles. Dairy Science & Technology, 2013. **93**(4): p. 357-371.
25. Hassenkam, T., et al., Tracking single coccolith dissolution with picogram resolution and implications for CO<sub>2</sub> sequestration and ocean acidification. Proceedings of the National Academy of Sciences, 2011. **108**(21): p. 8571-8576.
26. Svanbäck, S., H. Ehlers, and J. Yliruusi, Optical microscopy as a comparative analytical technique for single-particle dissolution studies. International Journal of Pharmaceutics, 2014. **469**(1): p. 10-16.
27. Svanbäck, S., et al., On-Chip Optofluidic Single-Particle Method for Rapid Microscale Equilibrium Solubility Screening of Biologically Active Substances. Analytical Chemistry, 2015. **87**(10): p. 5041-5045.
28. Prasad, K.V.R., et al., Dissolution kinetics of paracetamol single crystals. International Journal of Pharmaceutics, 2002. **238**(1): p. 29-41.
29. Raghavan, S.L., et al., *Dissolution Kinetics of Single Crystals of  $\alpha$ -Lactose Monohydrate*. Journal of Pharmaceutical Sciences, 2002. **91**(10): p. 2166-2174.
30. Østergaard, J., et al., Monitoring lidocaine single - crystal dissolution by ultraviolet imaging. Journal of Pharmaceutical Sciences, 2011. **100**(8): p. 3405-3410.
31. Pedersen, P.V. and K.F. Brown, Experimental Evaluation of Three Single - Particle Dissolution Models. Journal of Pharmaceutical Sciences, 1976. **65**(10): p. 1442-1447.
32. Dali, M.V. and J.T.P. Carstensen, Effect of Change in Shape Factor of a Single Crystal on Its Dissolution Behavior. Pharmaceutical Research, 1996. **13**(1): p. 155-162.

33. Simões, S., L. Pereira de Almeida, and M. Figueiredo, Testing the applicability of classical diffusional models to polydisperse systems. *International Journal of Pharmaceutics*, 1996. **139**(1): p. 169-176.
34. Horkovics-Kovats, S., Dissolution and coarsening of polydisperse, polymorph drug particles liberated from a disintegrating finished dosage form: Theoretical considerations. *European Journal of Pharmaceutical Sciences*, 2016. **91**: p. 265-277.
35. Shekunov, B. and E.R. Montgomery, Theoretical Analysis of Drug Dissolution: I. Solubility and Intrinsic Dissolution Rate. *Journal of Pharmaceutical Sciences*, 2016. **105**(9): p. 2685-2697.
36. Wang, J. and D.R. Flanagan, General solution for diffusion-controlled dissolution of spherical particles. 1. Theory. *Journal of Pharmaceutical Sciences*, 1999. **88**(7): p. 731-738.
37. Dali, M.V. and J.T. Carstensen, Effect of Change in Shape Factor of a Single Crystal on Its Dissolution Behavior. *Pharmaceutical Research*, 1996. **13**(1): p. 155-162.
38. Siepmann, J. and F. Siepmann, Mathematical modeling of drug dissolution. *International Journal of Pharmaceutics*, 2013. **453**(1): p. 12-24.
39. Štěpánek, F., Computer-Aided Product Design: Granule Dissolution. *Chemical Engineering Research and Design*, 2004. **82**(11): p. 1458-1466.
40. Ansari, M.A. and F. Stepanek, Design of granule structure: Computational methods and experimental realization. *AIChE Journal*, 2006. **52**(11): p. 3762-3774.
41. Ansari, M.A. and F. Stepanek, The effect of granule microstructure on dissolution rate. *Powder Technology*, 2008. **181**(2): p. 104-114.
42. Kimber, J.A., S.G. Kazarian, and F. Štěpánek, Microstructure-based mathematical modelling and spectroscopic imaging of tablet dissolution. *Computers & Chemical Engineering*, 2011. **35**(7): p. 1328-1339.
43. Smrčka, D., J. Dohnal, and F. Štěpánek, Effect of process scale-up on the dissolution of granules with a high content of active pharmaceutical ingredient. *Powder Technology*, 2015. **285**: p. 88-95.
44. Jia, X. and R.A. Williams, A Hybrid Mesoscale Modelling Approach to Dissolution of Granules and Tablets. *Chemical Engineering Research and Design*, 2007. **85**(7): p. 1027-1038.
45. Yuan, Q., X. Jia, and R.A. Williams, Validation of a multi-component digital dissolution model for irregular particles. *Powder Technology*, 2013. **240**: p. 25-30.
46. Guan, Y., et al., Lattice Boltzmann simulation of flow past a non-spherical particle. *Advanced Powder Technology*, 2017. **28**(6): p. 1486-1494.
47. Derksen, J.J., Simulations of solid-liquid mass transfer in fixed and fluidized beds. *Chemical Engineering Journal*, 2014. **255**: p. 233-244.
48. Derksen, J.J., et al., Simulations of dissolution of spherical particles in laminar shear flow. *Chemical Engineering Research and Design*, 2015. **93**: p. 66-78.
49. Babenko, Y.I. and E.V. Ivanov, Influence of non-steady-state effects on the dissolution rate of a single particle. *Theoretical Foundations of Chemical Engineering*, 2013. **47**(6): p. 687-692.
50. Crank, J., *The Mathematics of Diffusion*. 1979: Clarendon Press.
51. Moreno-Atanasio, R., R.A. Williams, and X. Jia, Combining X-ray microtomography with computer simulation for analysis of granular and porous materials. *Particuology*, 2010. **8**(2): p. 81-99.

52. Lowell, S., et al., *Characterization of Porous Solids and Powders: Surface Area, Pore Size and Density*. 2006: Springer Netherlands.
53. Koganti, V., et al., *Application of Modeling to Scale-up Dissolution in Pharmaceutical Manufacturing*. *AAPS PharmSciTech*, 2010. **11**(4): p. 1541-1548.

Figure 1  
[Click here to download high resolution image](#)

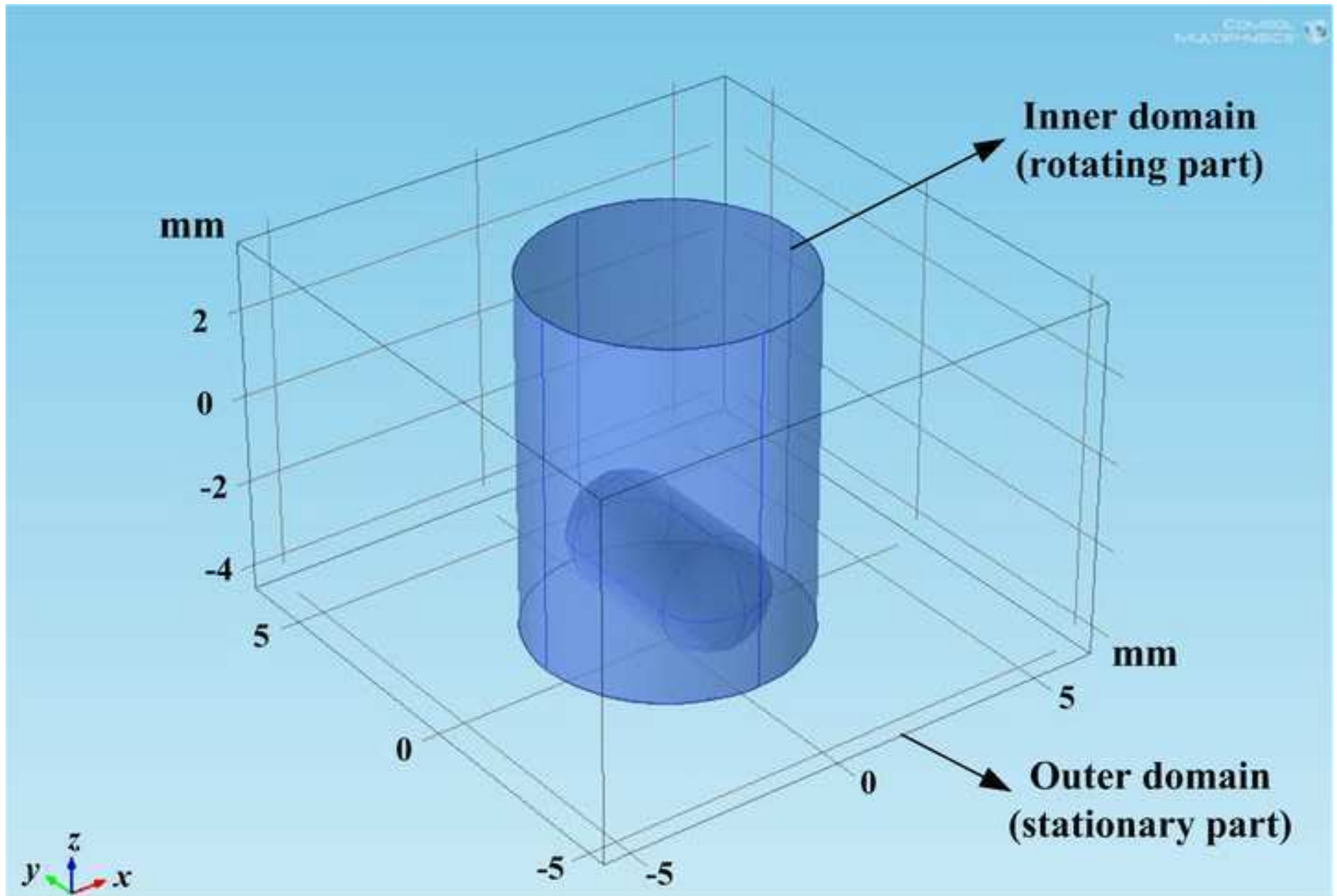


Figure 2  
[Click here to download high resolution image](#)

$$J = u_x A \left( \frac{C_{i-1} + C_i}{2} \right) + D_i A \left( \frac{C_{i-1} - C_i}{\Delta x} \right)$$

$$J = K_{i-1} A (C_{i-1}^S - C_i)$$

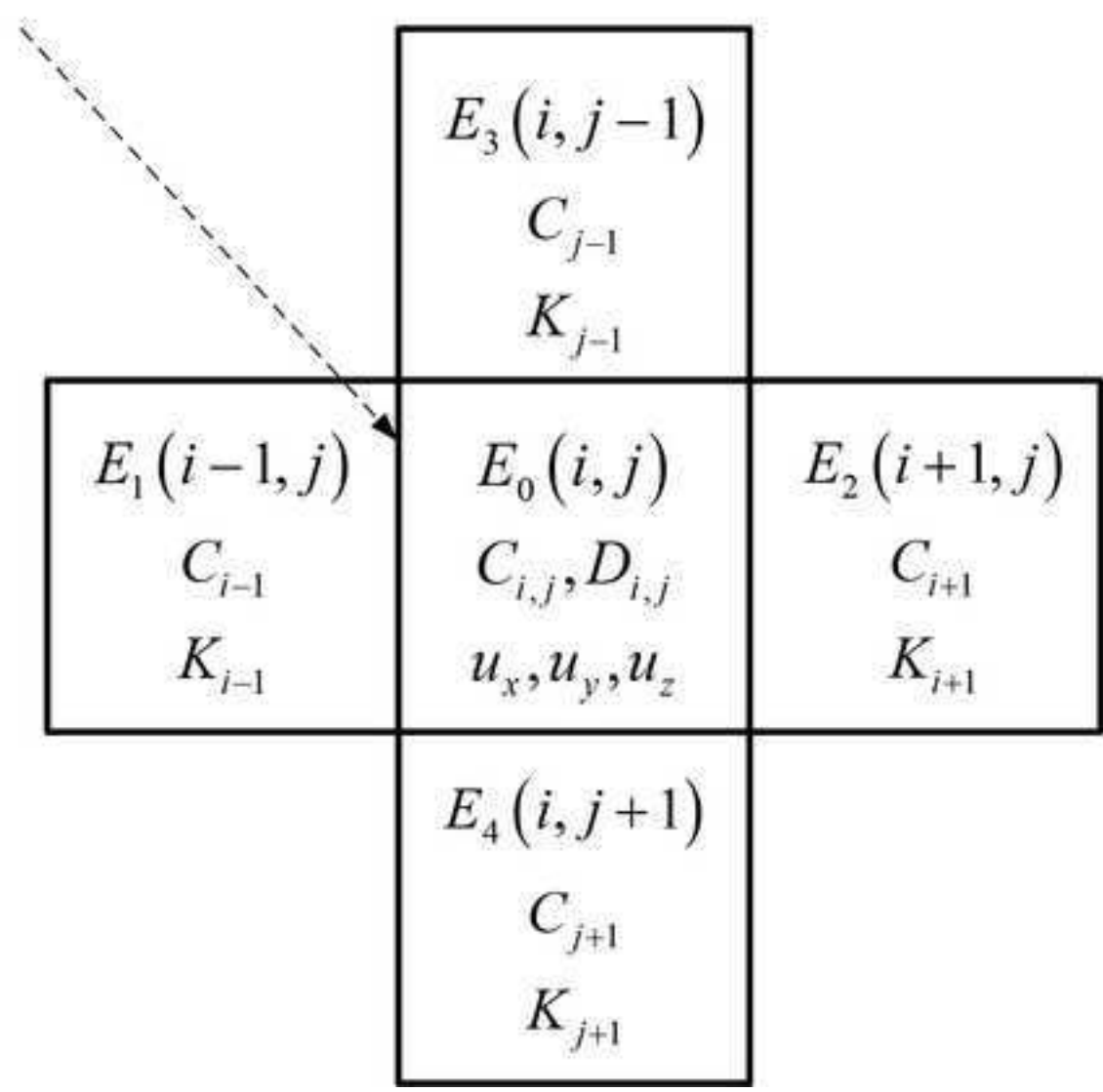


Figure 3  
[Click here to download high resolution image](#)

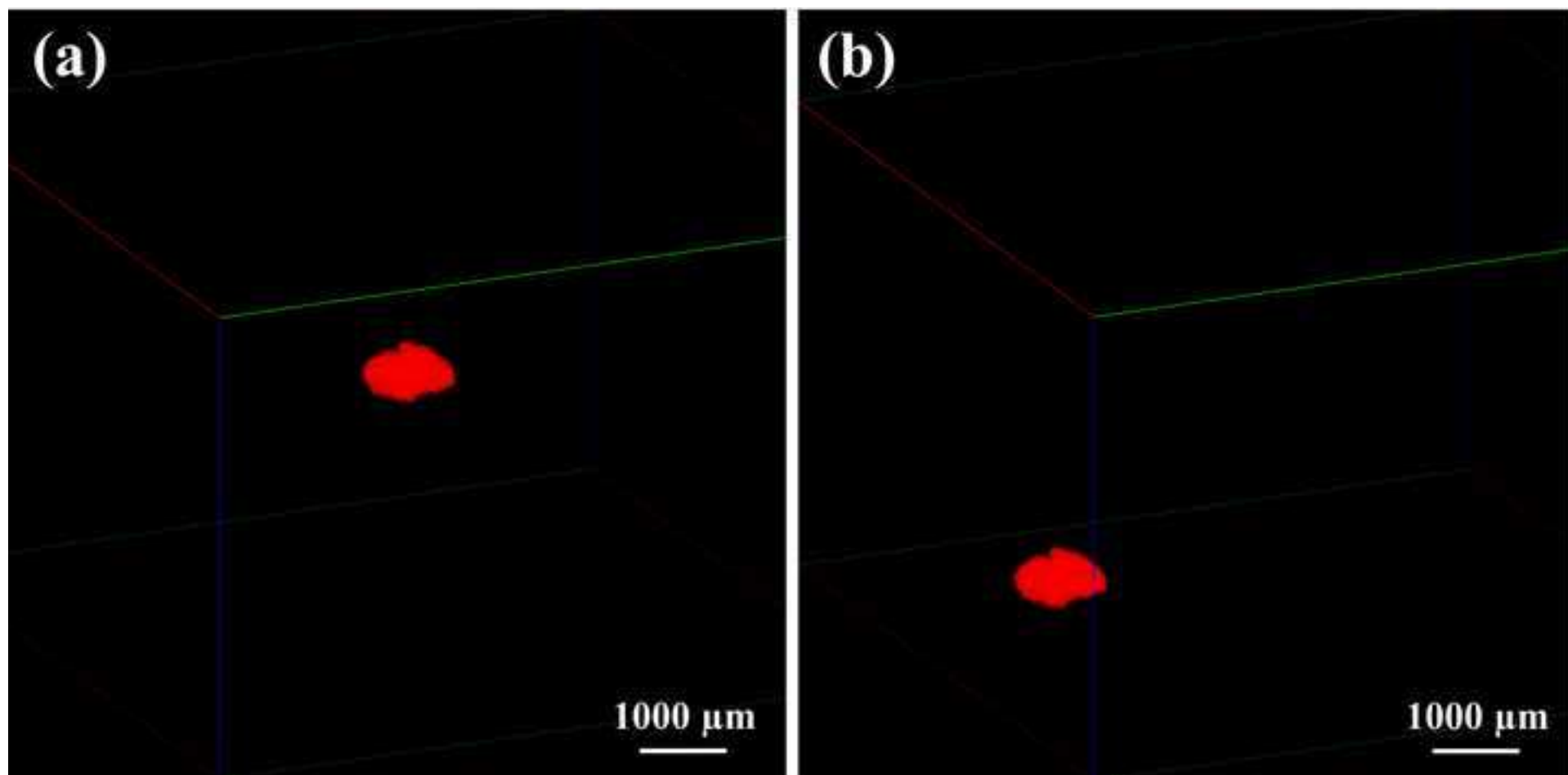
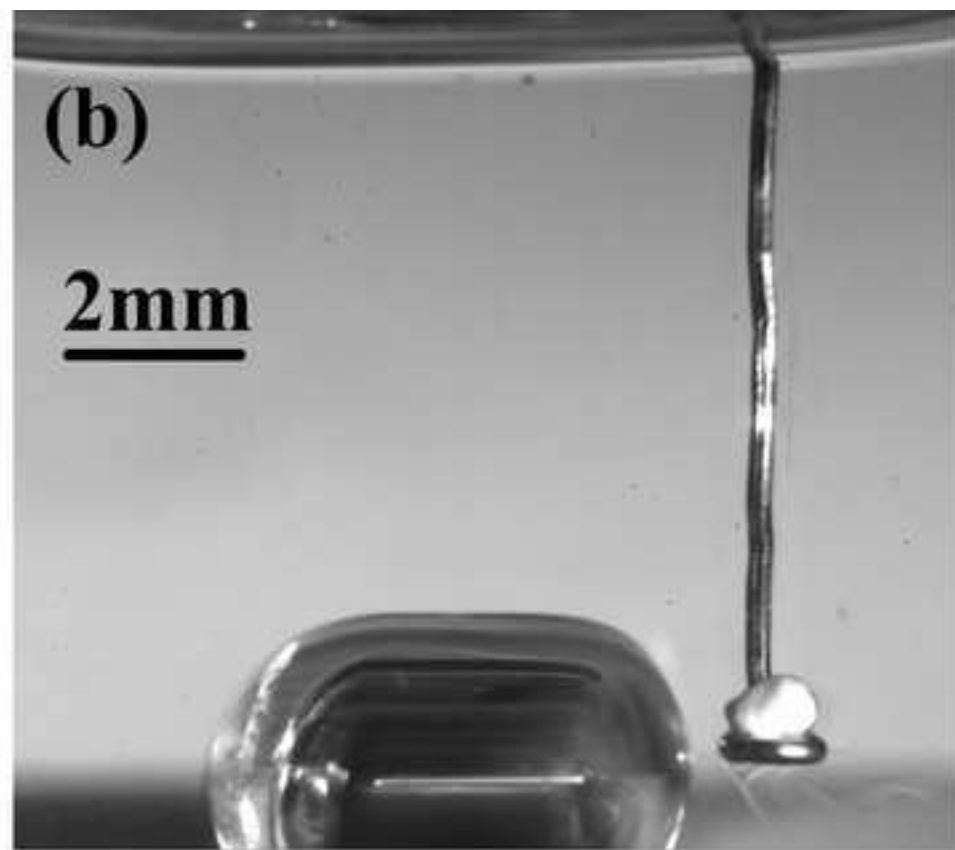
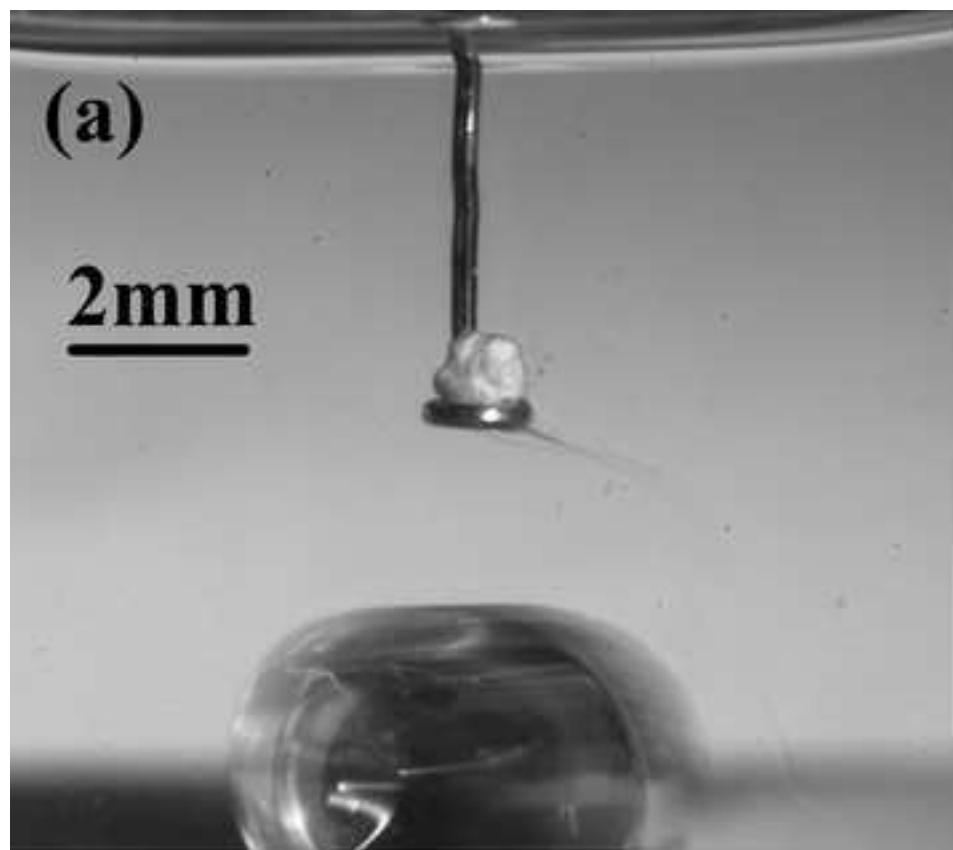


Figure 4  
[Click here to download high resolution image](#)



**Figure 5**  
[Click here to download high resolution image](#)

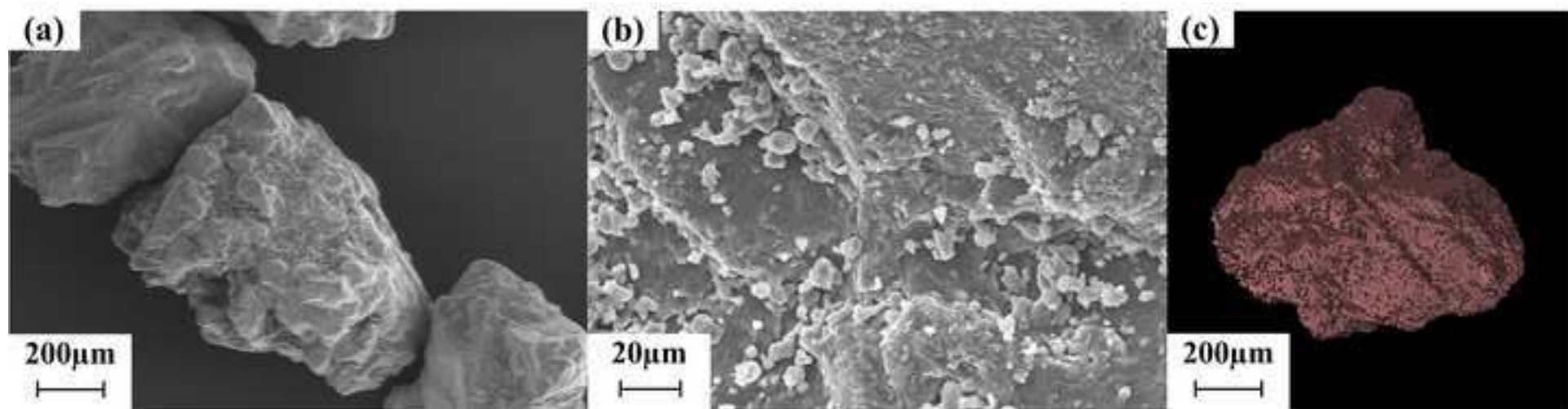


Figure 6  
[Click here to download high resolution image](#)

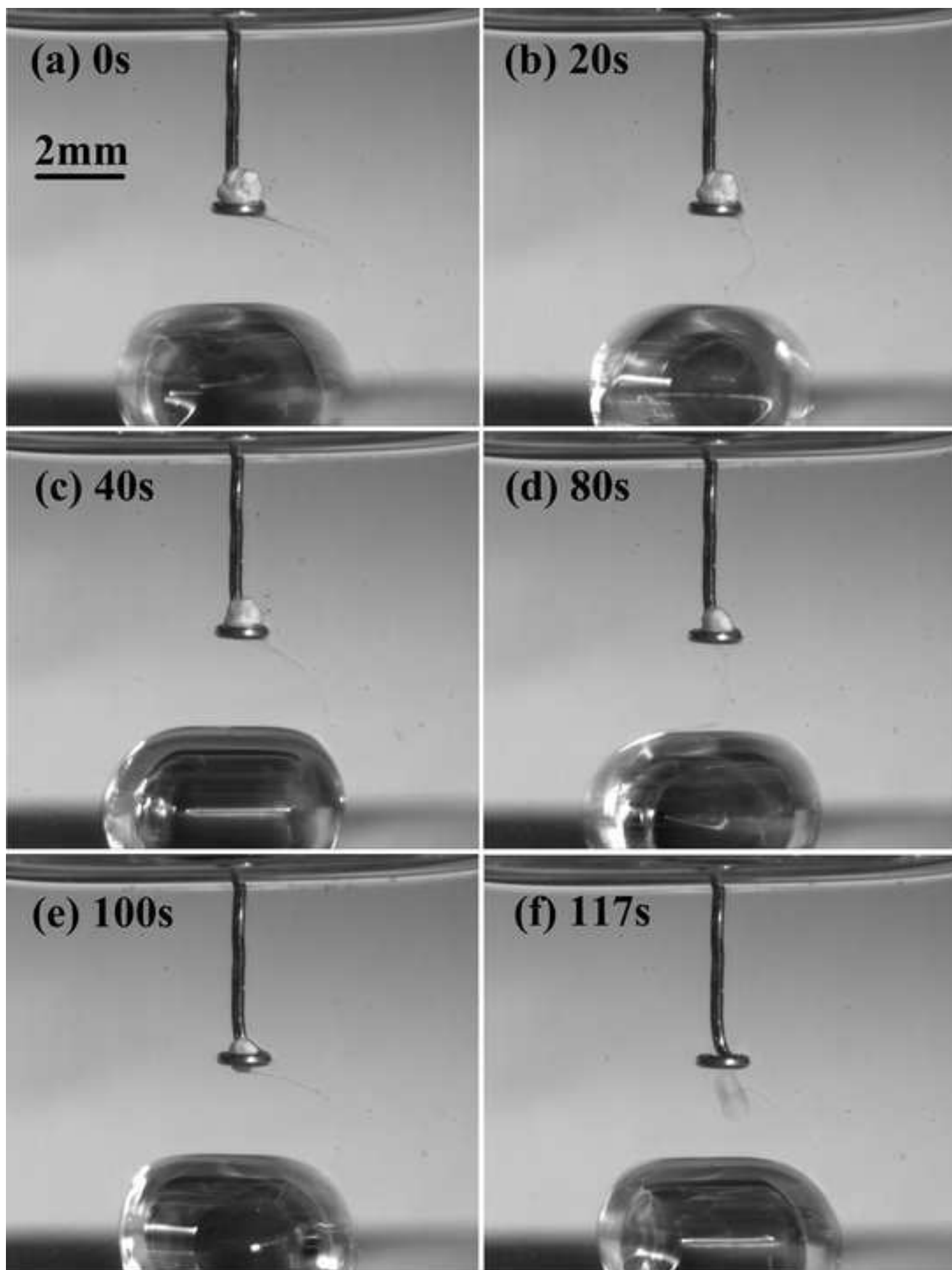


Figure 7  
[Click here to download high resolution image](#)

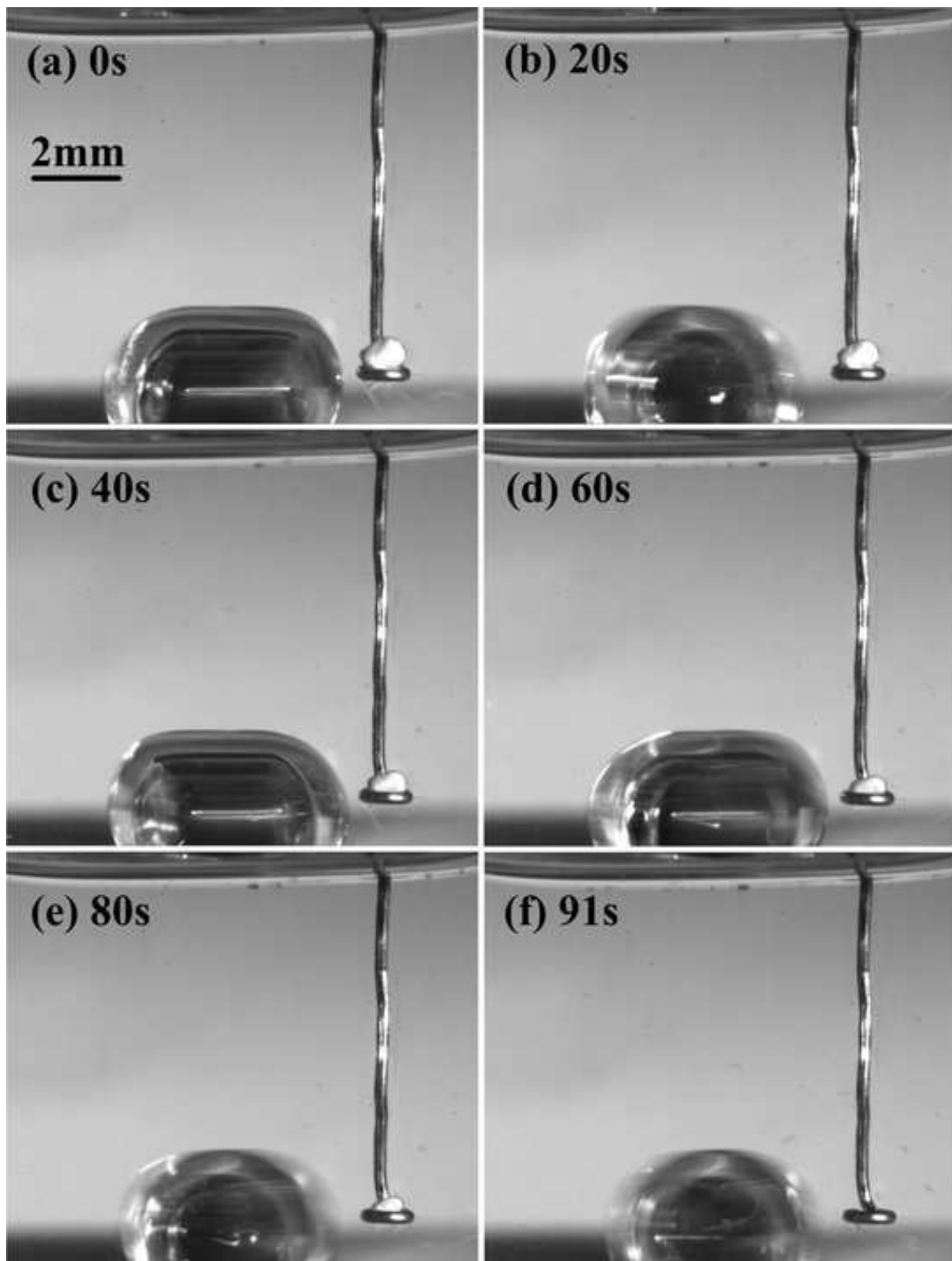


Figure 8  
[Click here to download high resolution image](#)

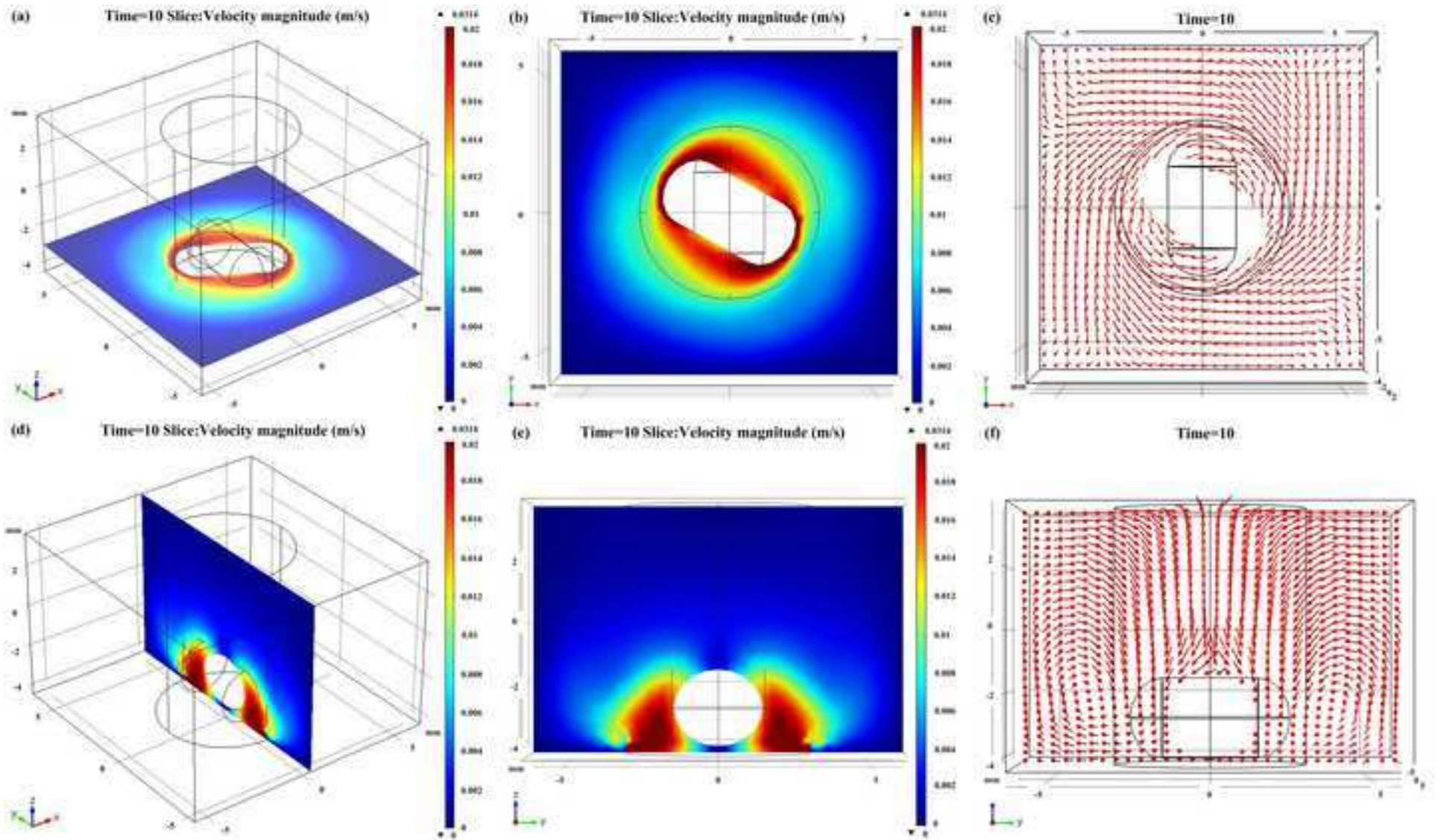


Figure 9  
[Click here to download high resolution image](#)

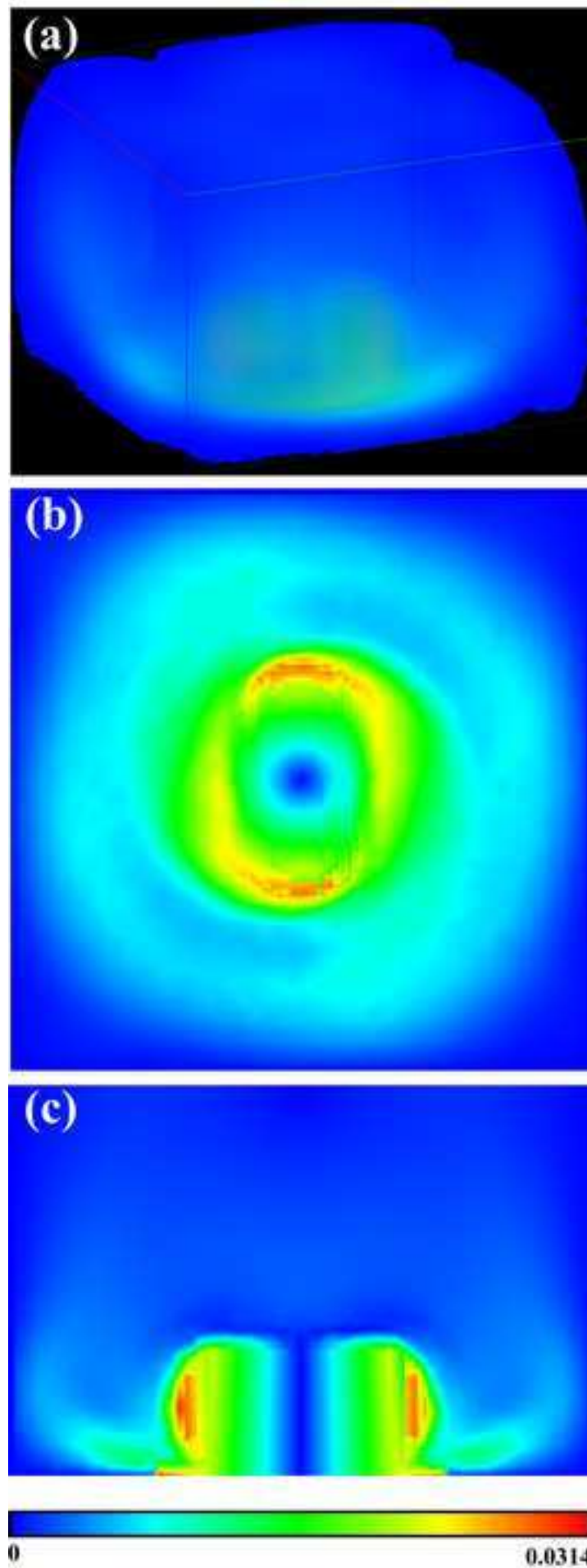


Figure 10  
[Click here to download high resolution image](#)

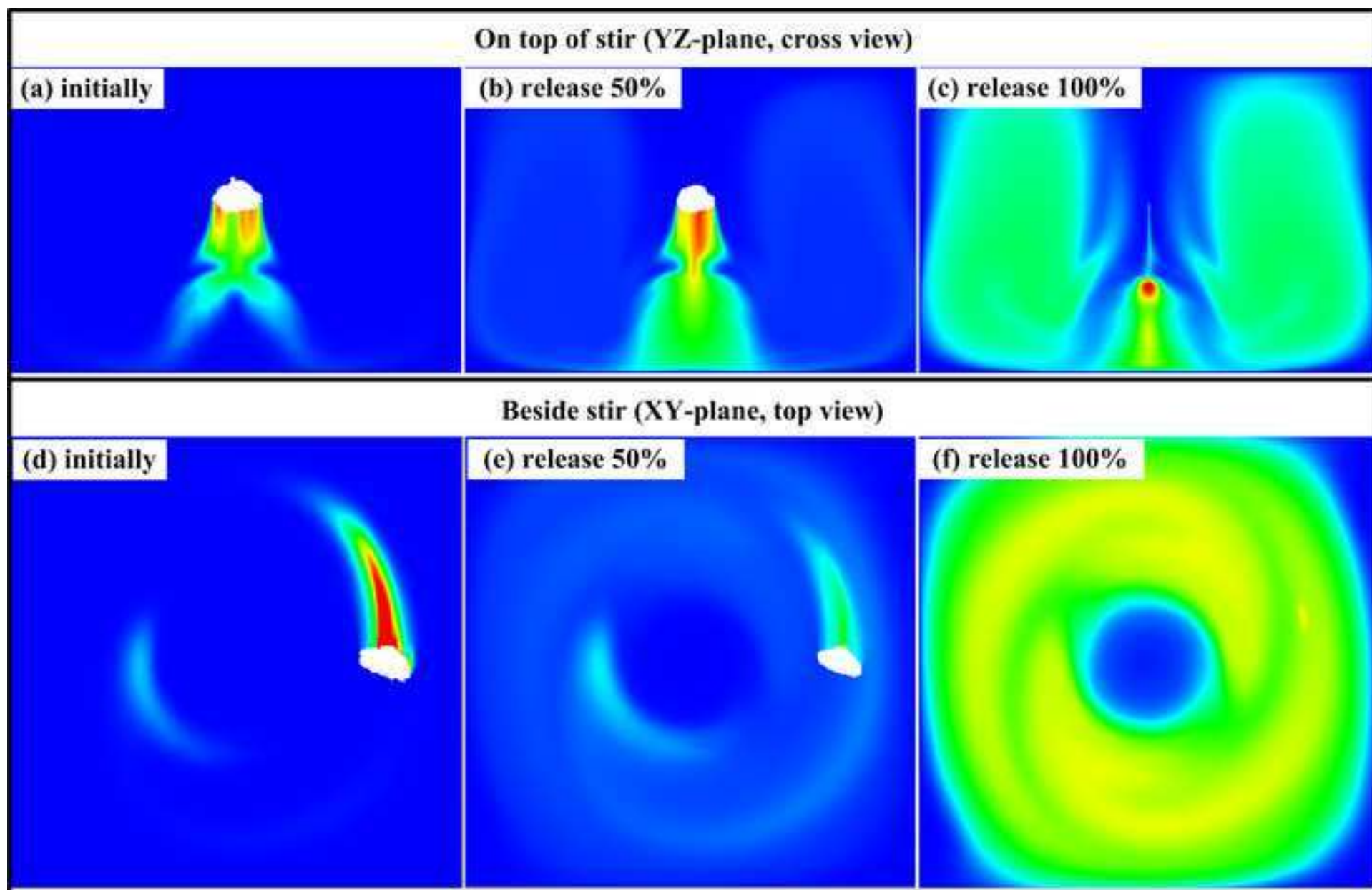


Figure 11  
[Click here to download high resolution image](#)

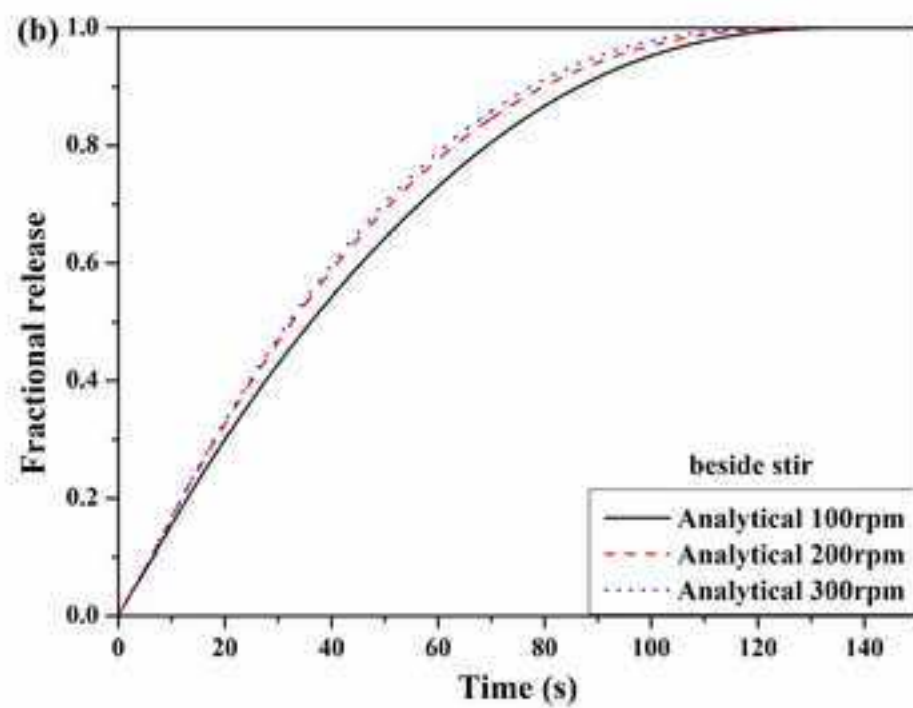
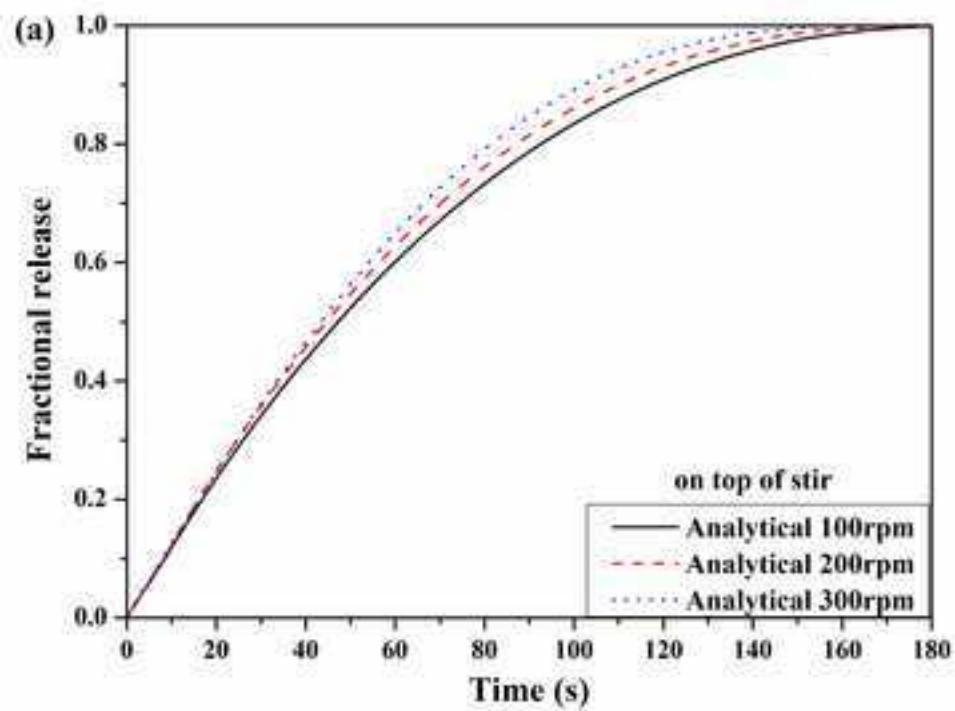


Figure 12a

[Click here to download high resolution image](#)

